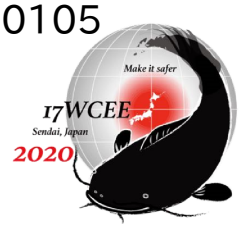

17th World Conference on Earthquake Engineering, 17WCEE
Sendai, Japan - September 13th to 18th 2020

SUPPLEMENTING SHEAR WAVE VELOCITY PROFILE DATABASE WITH MICROTREMOR-BASED H/V SPECTRAL RATIOS

T. Gospe[1], P. Zimmaro[2] ,S.K. Ahdi[3], A.Yong[4], P. Wang [5], T. Buckreis [6], S. Brandenberg [7], J.P. Stewart[8]

[1] *Graduate Student Researcher, University of California, Los Angeles, tbgospe@g.ucla.edu*
[2] *Project Scientist and Lecturer, University of California, Los Angeles, pzimmaro@ucla.edu*
[3] *Associate, Exponent, Inc.; Lecturer, University of California, Los Angeles, sahdi@ucla.edu*
[4] *Research Geophysicist, United States Geological Survey, Pasadena, yong@usgs.gov*
[5] *Graduate Student Researcher, University of California, Los Angeles, wltcwpf@g.ucla.edu*
[6] *Graduate Student Researcher, University of California, Los Angeles, tristan.buckreis@live.com*
[7] *Professor, University of California, Los Angeles, sjbrandenberg@ucla.edu*
[8] *Professor, University of California, Los Angeles, jstewart@seas.ucla.edu*

Abstract

Frequency-dependent horizontal-to-vertical (H/V) spectral ratios (HVSR) can provide information on one or more site resonant frequencies and relative levels of amplification at those frequencies. Such information is useful for predicting site amplification but is not present in site databases that have been developed over the last 15–20 years for the Next-Generation Attenuation (NGA) projects, which instead use the time-averaged shear-wave velocity (V_S) in the upper 30 m of the site (V_{S30}) as the primary site parameter and are supplemented with basin depth terms where available.

In order for H/V-based parameters to be used in future versions of site databases, a publicly accessible repository of this information is needed. We adapt a relational database developed to archive and disseminate V_S data to also include H/V spectra. Our intent with the database is to provide relevant H/V data and supporting metadata, but not parameters derived from the data. We consider the relevant data to be the frequency-dependent HVSR, where the horizontal component is taken from the geometric mean of as-recorded azimuths. Relevant metadata includes site location information, details about the equipment used to make the measurements, and processing details related to windowing, anti-trigger routines, and filtering. We describe the database schema developed to organize and present this information.

We also describe and illustrate routines that can be used to derive parameters from the data that are implemented in Python on a Jupyter Notebook enabled by DesignSafe-CI. These routines compute H/V spectral ratios based on the median horizontal component, and polar plots that present azimuthal dependence of spectra. For median-component spectra, additional routines fit pulse functions that provide frequency, amplitude, and pulse width parameters. These routines interact with the database via cloud computing, but are not directly part of the database.

Keywords: horizontal-to-vertical spectral ratios, resonant frequencies, site response, relational database

1. Introduction

Seismic site response is influenced by several factors, including: resonance, nonlinearity, amplification due to impedance contrasts, and amplification related to wave propagation in sedimentary basins. Ground-motion models predict site response conditioned on relatively simple site parameters such as the time-averaged shear wave velocity (V_S) to 30 m depth (V_{S30}) and depth to the 1 km/s or 2.5 km/s V_S [1]. These models are referred to as ergodic [2], even if the site parameters are measured on site. The underlying models are ergodic because they are derived from large global or regional databases, and as such are not site-specific.

Any particular site would be expected to produce site amplification that departs from the ergodic estimate for a variety of reasons related to location-specific geologic conditions. A site amplification model that accounts for the effects of these features on site amplification is non-ergodic [e.g., 3]. One common feature of non-ergodic site response is resonance at one (fundamental site frequency, f_0) or more site frequencies (f_d) [4,5,6], which produce peaks that are smoothed out in ergodic models. The use of the horizontal-to-vertical (H/V) component Fourier amplitude vs. frequency plots have the potential to add this site-specific attribute to predictions of ergodic site response at low cost, relative to non-ergodic procedures. While V_{S30} provides a reasonable, first-order estimate of site response over a wide frequency range [7,8,9], f_0 can be effective at describing site amplification for frequencies proximate to f_0, but it has limited utility elsewhere. Hence, the two parameters serve different purposes and we postulate that they can be most effectively utilized together [10,11]. This paper concerns the development of a database to store horizontal-to-vertical spectral ratios (HVSR) data. The database includes the raw data as-recorded signals in the time domain and the processing parameters used to derive the spectral ratios.

Many previous studies, mostly considering data from Europe, Japan, and central and eastern North America, have investigated the use of HVSR, which have generally proven to be effective at identifying the peak frequency associated with resonance effects, but inconclusive about the levels of site amplification that should be used [10,12,13,14,15].

This paper describes the extension of a V_S profile database (PDB), an early version of which is described by Ahdi et al. [16], to incorporate HVSR data. In this paper, we present a schema for the HVSR components of the database, where we explain the information that is stored and the results that can be readily extracted for ground motion studies. To place the schema in context, we explain the data acquisition process, the data processing procedures, procedures used to compute HVSR from the data, and external (to the database) routines that can be used to evaluate HVSR-related parameters used for site response studies.

2. Data Sources

While in California around 1,700 V_S profiles are publicly available via the PDB, fewer data exist for microtremor recordings [16]. One major source of HVSR data for strong motion stations is presented by Yong et al. [17]. The study (aka: American Recovery and Reinvestment Act funded project; hereafter as ARRA project) presents data from 191 strong-motion stations, the majority of which are located in California (187 stations), with an additional four stations in the central and eastern United States. Additionally, we have data from 33 sites in the Sacramento-San Joaquin Delta acquired by the coauthor T. Buckreis.

The California Strong Motion Instrumentation Program (CSMIP), part of the California Geological Survey (CGS), funded various studies to characterize ground motion recording station sites in California. A total of 12, 13, and 15 HVSR are available from the following CSMIP-funded reports: GEOVision [18], Petralogix [19], and GEOVision [20], respectively. These CSMIP reports have not yet been added to the database.

Using the data currently incorporated into the PDB, Figure 1 shows the relative number of V_S profiles and HVSR sites in California. Whereas various techniques have been used to collect profile data since the 1960s, the collection of microtremor data that is publicly accessible is much more recent.

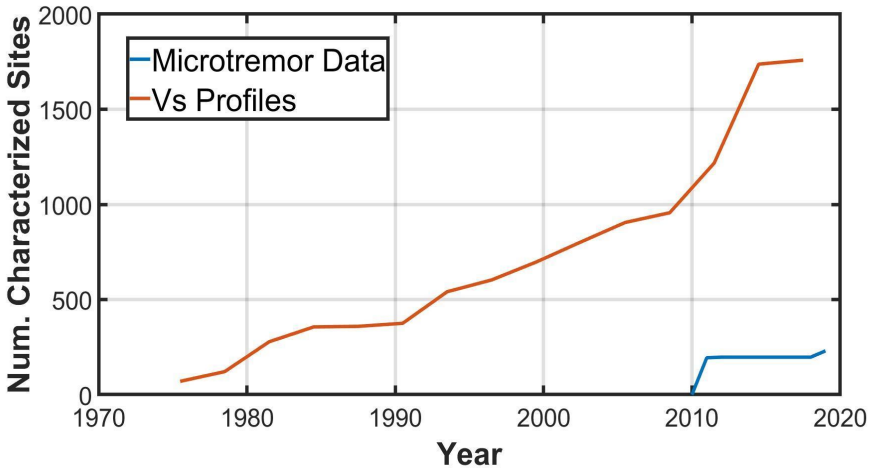

Figure 1 – Cumulative distribution of Vs profiles and microtremor data in California versus time.

The database is structured to allow entry of HVSR data from three sources: microtremor array measurements (MAM) [17, 21], pre-event noise from three-component earthquake seismograms, and seismic signals [21]. Data from earthquakes and pre-event noise come from triggered instruments, whereas we use continuous instruments to collect MAM data. MAM data is preferred because it matches the data type that would generally be used in forward applications. Comparisons of HVSR from seismograms to those from MAM indicate that in many cases good matches are obtained [21,22]. However, the matches are not always favorable, and the conditions that give rise to poor matches are poorly understood. Figure 2 shows an example of HVSR data for a site in the California Bay-Delta region (YU_HOL2), including pre-event noise, an earthquake ("Seismic Event"), and MAM recordings. The MAM data indicates a peak frequency at about 4 Hz, whereas for other sources the frequency is lower and the peak amplitudes are reduced.

As the database grows, we plan to include HVSR data from MAM and pre-event noise data, to facilitate further research on differences in spectral ratios and the causes of those differences.

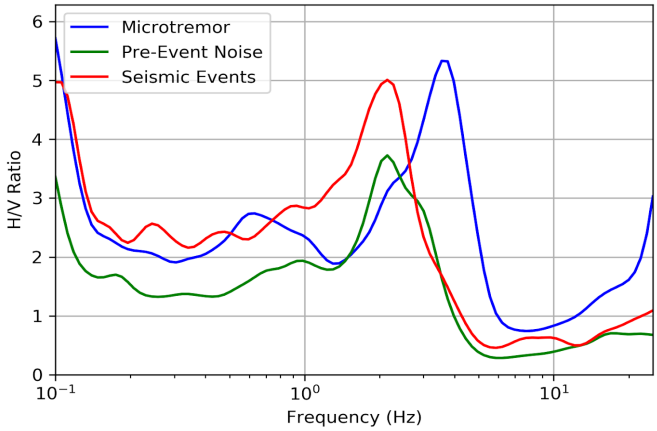

Figure 2 – Computed HVSR data from three sources for a site in the Delta (YU_HOL2): microtremor, pre-event noise, and seismic events.

As discussed above, the microtremor data in the current PDB consists of 191 ARRA project sites and 33 Delta sites. Using the Incorporated Research Institutions for Seismology (IRIS) database, we have obtained recordings from which pre-event noise can be extracted and then used to evaluate HVSR for 700 sites, and the process of adding more is ongoing. The instruments we use from IRIS are high-gain seismometers and an accelerometer with bandwidths between 80-250 Hz. Figure 3 depicts the ultimate site inventory in the database, which includes 224 sites from microtremor (green and pink dots) and 700 sites from pre-event noise (white-circles).

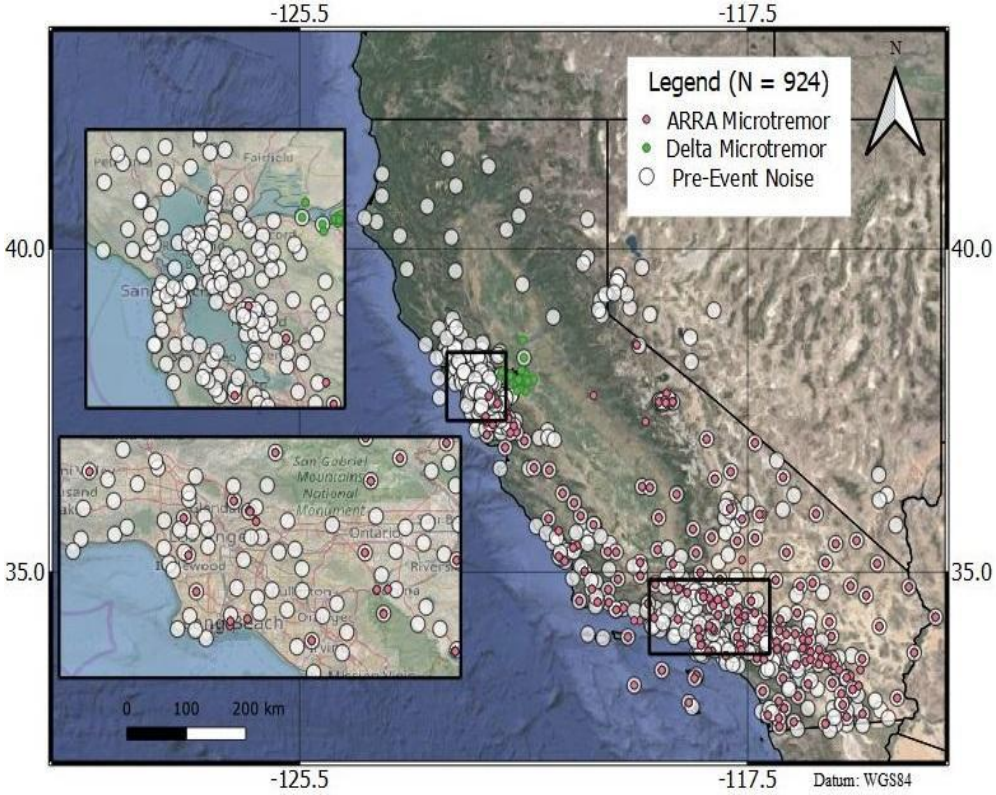

Figure 3 – Locations of sites in PDB with HVSR from either pre-event noise or microtremor sources.

3. Processing Parameters

This section describes the processing procedures that have been adopted to convert time-domain signals from triaxial seismometers or accelerometers to HVSR. These procedures borrow heavily from **S**ite **E**ffect**S** assessment using **AM**bient **E**xcitations (SESAME) guidelines [23] and protocols often used in California (K. Hayashi, A. Martin, oral and written personal communication, 2018, 2019). Geopsy [24] is the most common platform used to process data in this database.

3.1 Microtremor Array Measurements (MAM)

3.1.1 Number of Windows and Cycles

The HVSR peak frequency should be greater than 10 divided by the window duration in seconds [23]. The total number of significant cycles is defined as $N_{cyc}=T_{win}f_0N_{win}$, where T_{win} is window length (in sec), f_0 is the frequency (in Hz) of the lowest prominent peak in the H/V spectrum, and N_{win} is the number of windows used in the H/V spectrum computation. It is good practice to have no fewer than 200 cycles in the time series used for H/V computation, which effectively sets a minimum signal duration ($T_{sig} = N_{cyc} / f_0$).

Table 1 shows typical values for the above parameters as provided in recommendations for H/V testing in SESAME guidelines [23]. It is important to note that parameters can be manipulated to ensure that the number of significant cycles stays larger than 200.

Table 1 – Recommended recording duration, assuming at least N_{cyc} = 200 and N_{win} = 10 [23].

f_0 [Hz]	Minimum value for T_{win} [s]	Recommended minimum record duration T_{sig} [s]
0.2	50	1800
0.5	20	1200
1	10	600
2	5	300
5	5	180
10	5	120

3.1.2 Window Overlap; Taper Width and Type of Window

Sometimes the signal duration is not long enough and the windows may be too short in duration to satisfy the suggested window lengths (Table 1). To adjust for this, time windows can overlap by a specified percentage [24]. We use cosine tapers with a length of 5% of the window length [25].

3.1.3 Anti-Triggering

"Triggering" refers to a temporary vibration source affecting a signal, which can compromise the accuracy of HVSR. It is preferred for the ground vibrations producing the signals to be from far-field noise sources that produce approximately constant amplitudes in time. In contrast, local noise will have transient bursts due to the erratic nature of traffic or other anthropogenic sources. Anti-triggering is used on both the raw and filtered signal [23] to remove intervals of the signal with potential triggers. The objective of anti-triggering is to ensure approximately constant amplitudes in time.

The presence of potential triggers within a window of the recorded signal is judged based on relative values of the short-term average (STA) and long-term average (LTA) signal amplitudes. The STA and LTA are computed using 5- and 30-sec durations, respectively. The SESAME guidelines call for the amplitude ratios to be within the range of STA/LTA = 0.1 to 10 [23].

During signal processing, we look for stationary (i.e., approximately constant amplitude) intervals of ambient vibrations. Removing windows with transient signal produces clearer peaks in HVSR curves and lowers the HVSR standard deviation. The anti-triggering algorithm is typically applied to both horizontal and vertical components.

While the anti-triggering algorithm can be applied to either the unfiltered or filtered noise signals, here we apply it to the raw (pre-filtered) signal (consistent with procedures used in Yong et al. [17]). Within the metadata table we provide STA duration, LTA duration, and the STA/LTA amplitude range.

3.1.4 Bad Sample Tolerance and Threshold

The bad sample tolerance and threshold options help the user optimize the number of windows [24]. The bad sample options allow windows to be selected that do not satisfy the anti-triggering criteria. The bad sample tolerance allows the user to define the number of bad samples which can remain in a useable window. The use of bad samples may be necessary if the available data do not allow the criteria in Table 1 to be met. Similarly, the bad sample threshold option allows the user to pick the total duration of bad signal in seconds that a window can have. The tolerance is expressed as a user-defined number of seconds, whereas the threshold is a percentage of the total points in a window.

3.1.5 Filter

Filtering is applied to reduce low-frequency drifts in waveforms. As such, filtering is performed to cut low-frequency portions of signals. The corner frequency applied for this filter depends on the sensor used for analysis and is chosen manually for each signal. Given the equipment used in the field deployments described in Section 2, the corner frequency is usually around 0.1 Hz. The corner frequency for each signal is recorded as metadata. The upper bound frequency is determined by the Nyquist frequency.

3.1.6 Smoothing Type and Constant

Smoothing of a signal is necessary to reduce high frequency noise and isolate the true signal and identify f_0 values. The Konno & Ohmachi [26] smoothing filter, which accounts for variable numbers of points at low frequency [23], is used. The degree of smoothing increases as the bandwidth decreases and smoothing is applied to the HVSR ratio for each window. Chatelain et al., [25] uses a bandwidth parameter of 40. We typically use a value of 30 and change this parameter depending on the quality of the data over the range of 20-40. Noisy data might need a lower bandwidth value.

3.1.7 Horizontal Component Combination Method

Because horizontal ground motions are recorded in two directions, some method of combining these components is required. In order to minimize data manipulation in the database, the geometric mean of the as-recorded horizontal azimuths is stored in the database. We include the geometric mean because this is the direct HVSR computation from Geopsy, and as such, no manipulation of the data is required. For engineering applications, we recommend the use of orientation-independent definitions of the horizontal component such as the median-component (RotD50) or quadratic mean of the horizontal Fourier spectra, both used in NGA projects for earthquake ground motions.

3.1.8 HVSR Calculation

HVSRs are computed as a function of frequency by dividing the geometric mean horizontal-component Fourier amplitudes by the vertical-component smoothed Fourier amplitudes. Section 5 describes routines that operate on information within the database to combine median-component HVSR and HVSR for various azimuths (every 10 degrees from true north to south). The uncertainties in HVSR ordinates are calculated as the standard deviation among the HVSR time windows.

3.2 Pre-event Noise

While ambient vibration recordings may be several hours long, pre-event noise is available in shorter durations for a particular record, and several such records may be available (one for each earthquake at the site). This is because pre-event noise are triggered data from strong motion stations, and these recordings ordinarily capture the seismic event and a few minutes of pre-event signal stored in instrument memory. Because of these differences in duration between pre-event noise and microtremor data, the processing steps discussed in Section 3.1 require modification. Here we present the main distinctions in HVSR analysis for pre-event noise.

We first obtain the data from a seismic ground motion data archive, such as IRIS [27]. Next, we identify the pre-event noise segment from each processed earthquake ground motion time series. Figure 4 illustrates the P-wave arrival and the selected window for HVSR analysis using pre-event noise. We identify the P-wave arrival time visually (figure 4).

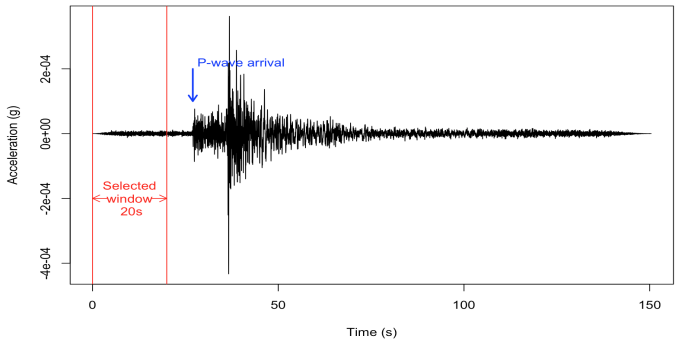

Figure 4 – Example of pre-event noise and P-wave arrival from IRIS earthquake strong motion data.

We repeat the above procedure for each available event at the site. Each event's pre-event noise is taken as the equivalent of a sub-window as used with MAM data processing. Per the SESAME guidelines in Table 1, ideally there would be at least 10 sub-windows (events), each with a minimum duration of 20 seconds (to resolve a peak frequency as low as 1 Hz). In practice, this is not always the case, which increases uncertainties in HVSRs evaluated using this method.

After the time windows are selected, HVSRs are computed as described in Section 3.1.8. Uncertainties are also computed.

4. Database Schema

For the V_s profile database (PDB), a relational database was adopted as the means by which to organize and archive information [16]. This project adds HVSR to the PDB, which requires the addition of some tables to the existing database schema. The database has been developed using the My Structured Query Language (MySQL) relational database management system. Within the natural hazards community, there are many examples of "databases" that consist of non-structured data collections presented in the form of spreadsheets or text files. Structured relational databases represent a different tool to store data. Relational databases have a hierarchical structure that defines relationships among different tables. Data are stored in tables in a series of fields (or columns). The tables within the database are linked together through primary and foreign keys. Primary keys represent unique identifiers of each entry in a table. Hence, one primary key can only be used once in each table. A foreign key is a field in one table used to identify a record in another table. Foreign keys are used to link different tables to each other. Relational databases were introduced by IBM employee E.F. Codd in 1970 [29], and some advantages include avoiding redundancy and null fields, consistency (information is entered only once), and security (if a database crashes, information is saved) [28,29].

The tables related to HVSR data in the PDB are listed in Table 2. The tables fall into two categories: general information and geophysical data. The meaning of the table names in Table 2 are described in subsequent subsections. Figure 5 shows all tables, specific fields, and the primary and foreign keys in each table.

Table 2 –Different group and table types and the number of fields in the HVSR schema.

Group Type	*Table Type*	*No. Fields*
General	site	18
	associated	6
	file	6
Geophysical	spectralRatioMeta	45
	meanCurve	5
	azimuthVariation	3
	polarCurve	4

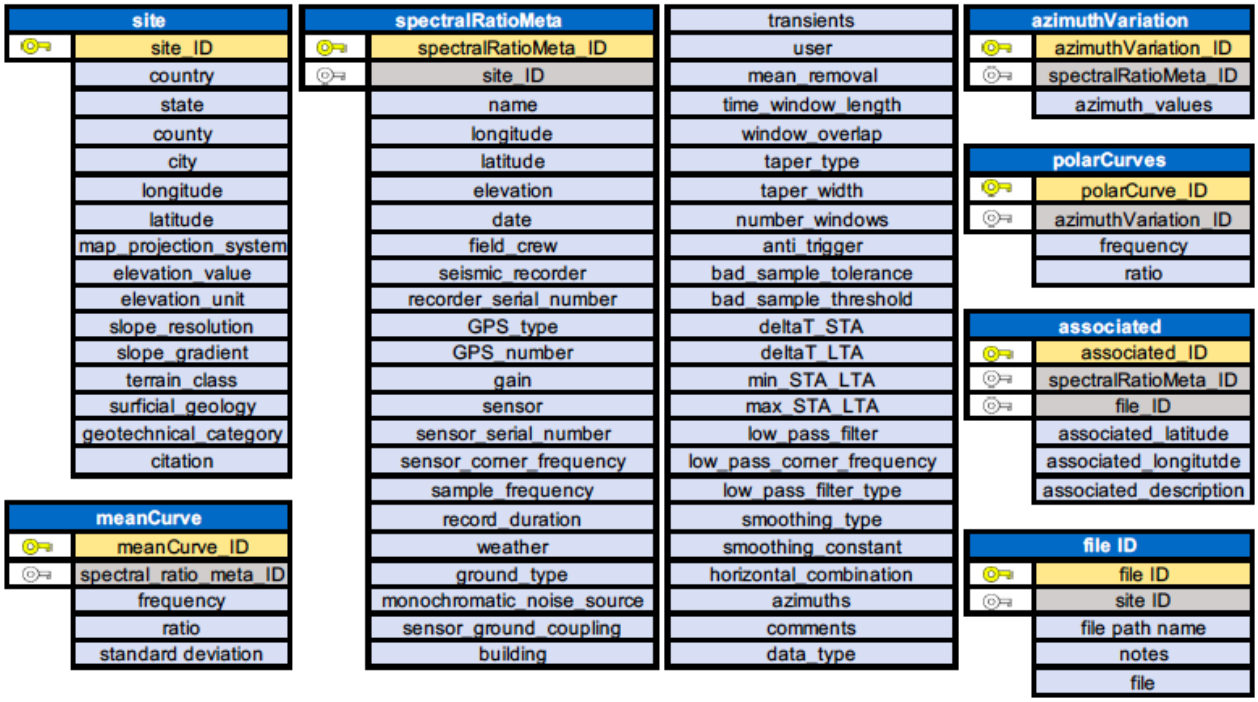

Figure 5 –Tables, fields, and primary (gold) and foreign (white) keys in HVSR database schema. Site table is taken from the V_S Profile Database schema developed by Ahdi et al. [30] and Sadiq et al. [31].

4.1 Metadata

The purpose of the spectralRatioMeta table (Figure 5) is to provide the user with the processing parameters used to produce the HVSR curves. Some of these columns may be null depending on the source for the HVSR curve, which is noted in the last column, data_type of Figure 5. The primary key is the spectralRatioMeta_ID and the foreign key is the site_ID field.

4.2 Mean Curve Table

The meanCurve table provides the geometric mean HVSR ordinates across all windows. The mean is computed for each frequency. The standard_deviation field is similarly computed using data from different time windows. For plotting purposes, we show the ratio of geometric mean HVSR and the mean +/- one standard_deviation (Figure 6). The primary key is the meanCurve_ID and the foreign key spectralRatioMeta_ID.

4.3 Azimuth Variation and Polar Curves Tables

The azimuthVariation includes azimuth values from 0 to 180 degrees in varying increments, typically around 5-10 degrees. The primary key and foreign key are the azimuthVariation_ID and spectralRatioMeta_ID, respectively. The polar curves table contains the curves (frequency, ratio) for the azimuthVariation values where the polarCurve_ID is the primary key and the azimuthVariation_ID is the foreign key. Polar curves are generated by rotating the two horizontal components at selected azimuths. In the database, we typically store HVSR polar curves at 10-degree intervals (i.e. 18 polar curves - 0-180 degrees - for each site). The purpose of the polarCurve is to store HVSR data as a function of azimuth. Polar curves are often used to detect sites where topographic features may produce amplification effects due to wave-field polarization [32].

4.4 Associated and File ID Tables

The associated table acts as a junction table between the file and spectralRatioMeta table, where the latitude and longitude refer to the location of pictures at the site. The primary key is the associated_ID and the foreign key is the spectralRatioMeta_ID. Lastly, the file_ID table provides the files used for data analysis as well as supplementary pictures or notes. For this table, the primary key is the file_ID and the foreign key is the site_ID.

5. Tools for Data Interpretation Outside of Database

The PDB provides plots of mean of geometric mean HVSR between time windows and tables showing azimuthal variations, but does not provide specific parameters derived from these results, such as might be used as site parameters to supplement V_{S30}. To facilitate such applications, the HVSR data archived in the relational database can be accessed via online Jupyter Notebook tools (example output in Figure 6). These tools interact with the data to interpret the data using protocols that have been applied in recent projects [3,31]. The interpreted parameters include (1) identification of features as peaks; (2) analysis of HVSR based on median horizontal components (RotD50); (3) plots of azimuthal variations of HVSR; and (4) for each peak in the median-component HVSR, fitting of a pulse function to evaluate peak frequency, peak amplitude, and width of peak. We envision that such post-processing tools will be used to analyze the data in the cloud without the need to download data locally.

Figure 6 shows an example of a microtremor HVSR spectral ratio measurement in the Sacramento-San Joaquin Delta. Site CE_67265 is located under a bridge between two piers. The peak is dominated by the bridge response in the azimuthal variation plot around 0 or 180 degrees (N-S direction).

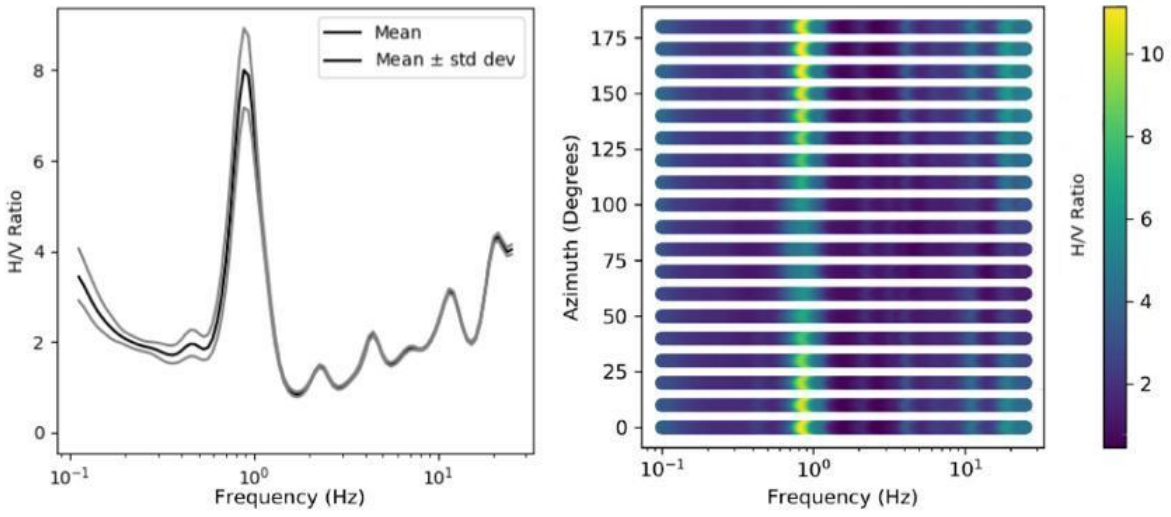

Figure 6 – A site in the Sacramento-San Joaquin Delta. Left:frequency versus H/V Ratio from a microtremor recording; right: azimuthal variation of the same recording.

HVSR plots can generally be classified as containing no peaks, one peaks, or multiple peaks [12]. If there are multiple peaks present, we take the first two peaks (i.e., the peak at the lower frequency). A peak generally indicates the site has strong impedance contrast(s) near one or more modal frequencies [e.g., 33] whereas multiple peaks may indicate multiple impedance contrasts at different depths. When there is no peak present in an HVSR, this suggests the site is either underlain with a sediment-filled depth profile that lacks a significant impedance contrast or it is a rock site with nearly depth-invariant near-surface velocities. To decide whether a feature in a plot such as Figure 6 is a peak or not, we require that the peak amplitude

exceed 2.0 and that its amplitude exceed 1.5 times the geometric mean of the HVSR curve [34]. For mean HVSR plots with a peak, we fit a Gaussian pulse function defined as follows [32, 35]:

$$\ln(F_{H/V,i}) = \ln(a_{pi}) \exp\left(-\left(\frac{ln(f/f_{pi})}{w_i}\right)^2\right) \quad (1)$$

where f_{pi} is the fitted at-peak frequency, a_{pi} is pulse amplitude, w_i represents pulse width, i is the order of peak, and f is frequency in Hz. This Gaussian pulse function estimates a pulse amplitude, frequency, and width for each peak. The nonlinear regression is performed in R using the Optim function by minimizing the sum of squared errors. Figure 7a demonstrates the fit of the pulse to data for Figure 6. Figures 7b-c show results for other sites with two peaks and no peaks, respectively. Table 3 lists the pulse-fitting parameters.

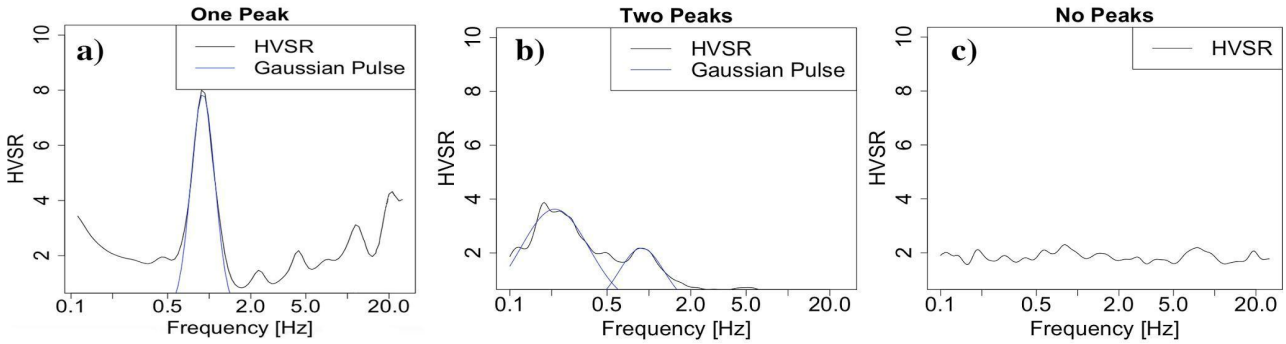

Figure 7 – HVSR spectral ratios versus frequency where the Gaussian pulse function is applied to sites on our database. The function identifies peaks of one, two, and no peaks for a (site CE.13929 sensor 507),b (site CE.11023 sensor 507), and c (site NC.BBGB sensor 453), respectively.

Table 3 – Categorizes the subwindows in Figure 7 and the following Gaussian pulse function parameters: pulse amplitude, width, and frequency.

Figure	*Number of Peaks*	a_{pi}	w_i	f_i *[Hz]*
7a	*0*	-	-	-
7b	*1*	*6.99*	*0.48*	*7.05*
7c	*2*	*3.63; 2.18*	*0.80; 0.53*	*0.21; 0.89*

6. Conclusions

We created an open-source relational database of HVSR and associated processing parameters and incorporate this information into an existing community V_s Profile Database (PDB) in the United States. Users can utilize and analyze the processed records through interactive Jupyter Notebook tools. The addition of the H/V site parameter is a valuable resource for future studies and will pave the way for H/V-based parameters to be included in the site database used in future NGA-type ground motion model development projects. We anticipate that this data will also prove useful over time for site-specific ground motion studies in the US.

7. Acknowledgments

Funding for this study is provided by California Strong Motion Instrumentation Program, California Geological Survey, Agreement 1016-985 and 1018-569. We gratefully acknowledge this support. We also thank Antony Martin from GEOVision for sharing his expertise on processing the HVSR data. Any use

of trade, firm, or product names is for descriptive purposes only and does not imply endorsement by the U.S. Government.

8. References

[1] Bozorgnia, Y., N. A. Abrahamson, L. .A. Atik, T. D. Ancheta, G. M. Atkinson, J. W. Baker, A. Baltay, D. M. Boore, K. W. Campbell, B. S.-J. Chiou, R. Darragh, S. Day, J. Donahue, R. W. Graves, N. Gregor, T. Hanks, I. M. Idriss, R. Kamai, T. Kishida, A. Kottke, S. A. Mahin, S. Rezaeian, B. Rowshandel, E. Seyhan, S. Shahi, T. Shantz, W. Silva, P. Spudich, J. P. Stewart, J. Watson-Lamprey, K. Wooddell, and R. Youngs, 2014. NGA-West 2 research project, *Earthq. Spectra*, **30**, 973-987.

[2] Anderson, J. G. and J. Brune, 1999. Probabilistic seismic hazard analysis without the ergodic assumption." *Seism. Res. Lett.*, **70**, 19-28.

[3] Stewart, J. P., K. Afshari, and C. A. Goulet, 2017. Non-ergodic site response in seismic hazard analysis, *Earthq, Spectra*, **33**, 1385-1414.

[4] Di Alessandro, C., L. F. Bonilla, D. M. Boore, A. Rovelli, and O. Scotti, 2012. Predominant-period site classification for response spectra prediction equations in Italy, *Bull. Seismol. Soc. Am.* **102**, 680–695.

[5] Bonilla, L.F., J. H. Steidl, J.-C. Gariel, and R.J. Archuleta (2002). Borehole response studies at the Garner Valley downhole array, Southern California, *Bull. Seismol. Soc. Am.* **92,** 3165-3179.

[6] Bonilla, L. F., J. H. Steidl, G. T. Lindley, A. G. Tumarkin, and R. J. Archuleta (1997). Site amplification in the San Fernando Valley, California: Variability of site-effect estimation using the S-wave, coda, and H/V methods, *Bull. Seismol. Soc. Am.* **87,** 710-730.

[7] Abrahamson, N. A., W. J. Silva, and R. Kamai (2014). Summary of the ASK14 ground motion relation for active crustal regions, *Earthq. Spectra* **30,** 1025-1055.

[8] Campbell, K. W., and Y. Bozorgnia (2014). NGA-West2 ground motion model for the average horizontal components of PGA, PGV, and 5% damped linear acceleration response spectra, *Earthq. Spectra* **30,** 1087-1115.

[9] Chiou, B. S.-J., and R. R. Youngs (2014). Update of the Chiou and Youngs NGA model for the average horizontal component of peak ground motion and response spectra, *Earthq. Spectra* **30,** 1117-11153.

[10] Cadet, H., P.-Y. Bard, A.-M. Duval, and E. Bertrand (2012). Site effect assessment using KiK-net data: Part 2—Site amplification prediction equation based on f0 and Vsz, Bull. Earthq. Eng. 10, 451–489.

[11] Gofrani, H., G.M. Atkinson, and K.Goda (2013). Implications of the 2011 M 9.0 Tohoku Japan earthquake for the treatment of site effects in large earthquakes, *Bull. Earthq. Eng.* **11,** 171-203.

[12] Kwak, D. Y., Stewart, J. P., Mandokhail, S. U. J., and Park, D. (2017). Supplementing VS 30 with H/V spectral ratios for predicting site effects. *Bull. Seismol. Soc. Am.* **107**, 2028-2042.

[13] Field, E. H., and K. H. Jacob (1993). The theoretical response of sedimentary layers to ambient seismic noise, *Geophys. Res. Lett.* **20**, 2925–2928.

[14] Theodulidis, N., R. J. Archuleta, P.-Y. Bard, and M. Bouchon (1996). Horizontal to vertical spectral ratio and geological conditions: The case of Garner Valley downhole array in southern California, *Bull. Seismol. Soc. Am.* **86**, 306–319.

[15] Kawase, H., Mori, Y., and Nagashima F. (2018). Difference of horizontal-to-vertical spectral ratios of observed earthquakes and microtremors and its application to S-wave velocity inversion based on the diffuse field concept. *Earth, Planets and Space*, **70**, 1.

[16] Ahdi, S.K., O. Ilhan, S. Sadiq, Y. Bozorgnia, Y.M.A. Hashash, D. Park, A. Yong, and J.P. Stewart (2018). Development of a United States Community Shear Wave Velocity Profile Database, *5th Conference on Geotechnical Earthquake Engineering and Soil Dynamics (GEESD-V)*, June 10–13, 2018, Austin, Texas.

[17] Yong, A, A Martin, KH Stokoe, and J Diehl, 2013, ARRA-funded VS30 measurements using multi-technique approach at strong-motion stations in California and central-eastern United States: U.S. Geological Survey Open-File Report 2013–1102, 59 p. and data files, http://pubs.usgs.gov/of/2013/1102/.

[18] GEOVision (2016). Surface Wave Measurements Report, Riverside County, California. Report 16192-01 Rev 2. Prepared for State of California Department of Conservation, California Geological Survey, Strong Motion Instrumentation Program.

[19] Petralogix (2017). Vs30 Site Characterization Report, Los Angeles, Orange, Ventura, San Bernardino, and Riverside Counties. Report 2017-00006.

[20] GEOVision (2018). Surface Wave Measurements, Santa Clara, Santa Cruz, San Benito, and Monterey Counties. Report 18045-01. Prepared for State of California Department of Conservation, California Geological Survey, Strong Motion Instrumentation Program.
[21] Hassani, B., Yong, A., Atkinson, G. M., Feng, T., and Meng, L. (2019). Comparison of site dominant frequency from earthquake and microseismic data in California. *Bull. Seismol. Soc. Am.*, **109(3),** 1034-1040.
[22] Satoh, T., H. Kawase, and S. Matsushima (2001). Differences between site characteristics obtained from microtremors, S-waves, P-waves, and codas, *Bull. Seismol. Soc. Am*. **91**, 313–334.
[23] SESAME, 2004, Guidelines for the Implementation of the H/V spectral ratio technique on ambient vibrations—Measurements, processing and interpretation: European Commission, Project No. EVG1-CT-2000-00026, accessed September 2012, at http://sesame-fp5.obs.ujf-grenoble.fr/
[24] Wathelet M. (2006). Geopsy Manual.
[25] Chatelain, J.-L., B. Guillier, B., Cara, F., Duval, A.-M., Atakan, K., Bard, P.-Y., and The WP02 SESAME team, (2008). Evaluation of the influence of experimental conditions on H/V results from ambient noise recordings, *Bull. Earthq. Eng,* **6**, 33–74.
[26] Konno, K., and Ohmachi, T. (1998). Ground-motion characteristics estimated from spectral ratio between horizontal and vertical components of microtremor. *Bull. Seismol. Soc. Am.* **88(1),** 228-241.
[27] "Incorporated Research Institutions for Seismology (IRIS), IRIS Earthquake Browser, http://ds.iris.edu/ieb/index.html, last accessed <01/07/2019>
[28] Brandenberg S.J., Zimmaro P., Stewart J.P., Kwak D.Y., Franke K.W., Moss R.E.S., Cetin K.O., Can G., Ilgac M., Stamatakos J., Weaver T., and Kramer S.L. (2019). Next Generation Liquefaction Database. *Earthq. Spectra*. In Press. DOI: 10.1177/8755293020902477.
[29] Codd, E. F. (1970). A relational model of data for large shared data banks. *Communications of the ACM*, *13*(6), 377-387.
[30] Ahdi, S. K. (2018). An Improved Framework for the Analysis and Dissemination of Seismic Site Characterization Data at Varying Resolutions. *UCLA*. ProQuest ID: Ahdi_ucla_0031D_17519. Merritt ID: ark:/13030/m54f6nxb. Retrieved from https://escholarship.org/uc/item/6p35w167
[31] Sadiq, S., O. Ilhan, S.K. Ahdi, Y. Bozorgnia, Y.M.A. Hashash, D. Park, A. Yong, and J.P. Stewart (2018). A Proposed Seismic Velocity Profile Database Model. *Eleventh U.S. National Conference on Earthquake Engineering (11NCEE)*, June 25–29, 2018, Los Angeles, California, Paper No. 1342.
[32] Di Giulio G., Cara F., Rovelli A., Lombardo G., and Rigano R. (2009). Evidences for strong directional resonances in intensely deformed zones of the Pernicana fault, Mount Etna, Italy. *Journal of Geophysical Research*, **114**, B10308.
[33] Tuan, T. T., F. Scherbaum, and P. G. Malischewsky (2011). On the relationship of peaks and troughs of the ellipticity (H/V) of Rayleigh waves and the transmission response of single layer over half-space models, *Geophys. J. Int*. **184**, 793–800.
[34] Hassani, B and GM Atkinson, 2016. Applicability of the site fundamental frequency as a V_{S30} proxy for Central and Eastern North America, *Bull. Seismol. Soc. Am.* **106**, 653–664.
[35] Ghofrani, H and GM Atkinson, 2014. Site condition evaluation using horizontal-to-vertical response spectral ratios of earthquakes in the NGA-West2 and Japanese databases, *Soil Dynam. Earthq. Eng.* **67**, 30–43.

